ACCSCIENCE PUBLISHING

International Journal of Bioprinting

RESEARCH ARTICLE

3D-printed amino acid-restricted foods for special medical purposes to support cancer nutrition therapy

Yuhao Wei[1†], Jiangfei Li[2†], Yuanyuan Chen[3†], Yu Xiang[1†], Guangqi Li[4], Yi-Ping Ho[5*], Xiaosheng Zhang[3*], Juan Huang[6*], Yi Zhang[3*], and Xuelei Ma[1*]

[1]Department of Biotherapy, State Key Laboratory of Biotherapy and Cancer Center, West China Hospital, Sichuan University, Chengdu, Sichuan, China

[2]Department of Food Nutrition and Health, School of Medicine and Health, Faculty of Life Sciences and Medicine, Harbin Institute of Technology, Harbin, Heilongjiang, China

[3]Intelligent Micro/Nano Circuits and Microsystems Integration Laboratory, School of Integrated Circuit Science and Engineering, University of Electronic Science and Technology of China, Chengdu, Sichuan, China

[4]Department of Radiation Oncology, Precision Radiation in Oncology Key Laboratory of Sichuan Province, Sichuan Clinical Research Center for Cancer, Sichuan Cancer Hospital & Institute, Sichuan Cancer Center, University of Electronic Science and Technology of China, Chengdu, Sichuan, China

[5]Department of Biomedical Engineering, Faculty of Engineering, The Chinese University of Hong Kong, Shatin, New Territories, Hong Kong SAR, China

[6]Department of Hematology, Sichuan Academy of Medical Sciences & Sichuan Provincial People's Hospital, University of Electronic Science and Technology of China, Chengdu, Sichuan, China

[†]These authors contributed equally to this work.

***Corresponding authors:**
Xuelei Ma
(maxuelei0726@wchscu.cn)
Yi Zhang
(yi_zhang@uestc.edu.cn)
Juan Huang
(huangjuanxy@med.uestc.edu.cn)
Xiaosheng Zhang
(zhangxs@uestc.edu.cn)
Yi-Ping Ho
(ypho@cuhk.edu.hk)

Citation: Wei Y, Li J, Chen Y, *et al*. 3D-printed amino acid-restricted foods for special medical purposes to support cancer nutrition therapy. *Int J Bioprint*. 2026:12(2):026060048. doi: 10.36922/IJB026060048

Received: February 4, 2026

Revised: February 25, 2025

Accepted: March 3, 2026

Published online: April 10, 2026

Abstract

Serine/glycine-free (−SG) diets are recognized for boosting tumor immunotherapy efficacy by remodeling the tumor microenvironment, yet their clinical translation is hindered by aspiration risks and poor patient compliance associated with traditional liquid formulations. To address these challenges, this study leveraged 3D printing to transform −SG nutritional powder into a clinically viable semi-solid formulation. A functional food ink was developed by stabilizing −SG powder in a hydrocolloid matrix formed via electrostatic complexation between cationic chitosan and anionic xanthan gum. Formulation was optimized using response surface design of experiment methodology to maximize printability, with metabolic efficacy and biological safety validated in BALB/c mice, and clinical usability assessed in 20 cancer patients via sensory and direct swallowing tests. Rheological characterization confirmed that the polyelectrolyte network endowed the ink with ideal pseudoplasticity and yield stress—critical for extrusion-based 3D printing. The optimized formulation (1.25% chitosan, 1.25‰ xanthan gum) exhibited exceptional shape fidelity. *In vivo* studies showed the 3D-printed food for special medical purposes maintained serum serine/glycine depletion without systemic toxicity, supported by stable mouse body weight and normal liver/kidney function. Clinically, the 3D-printed semi-solid formulation significantly enhanced patient compliance, elevating sensory acceptability scores from "like slightly" to "like very much" (32.0 vs. 27.6, $p < 0.0001$). This study presents a novel application of 3D printing to fabricate texture-modified food for special medical purposes, effectively mitigating aspiration risks associated with traditional liquid amino acid-restricted diets.

Keywords: 3D food printing; Food for special medical purposes; Tumor metabolism; Polyelectrolyte complex; Personalized nutrition

1. Introduction

Amino acids serve as building blocks for proteins and as substrates for biosynthetic processes.[1,2] Disorders of amino acid metabolism are associated with multiple diseases. The deletion of tumor suppressor genes, including *PTEN* and *TP53*, or the activation of oncogenic MYC and RAS signaling, can lead to alterations in nutrient supply, metabolic enzymes, metabolic requirements, and various other metabolic characteristics. Targeting tumor cell metabolism therapeutically has demonstrated effectiveness with reduced side effects relative to certain conventional treatments.[3,4] Furthermore, therapies targeting amino acid metabolism, including dietary restriction of the non-essential amino acids serine and glycine, have demonstrated therapeutic potential in murine models.[5] Tumors are likely dependent on an external supply of non-essential amino acids[6] Recent advancements in three-dimensional (3D) food printing have demonstrated significant potential in clinical nutrition. For instance, Pant *et al.*[7] successfully utilized food hydrocolloids to print fresh vegetables, improving visual appeal and texture for dysphagic patients. However, these studies primarily focused on physical texture modification or general metabolic disorders. There remains a critical lack of research on applying 3D printing to precision metabolic cancer therapy, specifically for fabricating amino acid-restricted functional foods that simultaneously meet metabolic therapeutic targets and swallowing safety requirements. Consequently, limiting these amino acids can impede tumor growth, highlighting the significance of amino acid metabolism.[8-18] Herein, we discuss the potential clinical application of the serine/glycine-free diet (−SG diet) in treating cancer.

In a previous study, we have developed the −SG diet nutritional powder and commenced a single-arm, phase I clinical trial of the −SG Diet for patients with advanced solid tumors.[5] Currently, there exists a challenge in nutritional therapy, whether focused on enhancing patients' nutritional status or supporting clinical treatment, because of the limited variety of available formulations. To transform the −SG nutritional powder into a printable ink with self-supporting capabilities, a precise hydrocolloid matrix is required. Chitosan and xanthan gum were specifically selected as the ink matrix not only for their status as generally recognized as safe food ingredients but also for their proven ability to form polyelectrolyte complexes. Chitosan, a cationic polysaccharide derived from chitin, was selected as the primary structural scaffold due to its biocompatibility and pH-responsive solubility. However, chitosan alone often lacks the requisite viscoelasticity for extrusion-based printing. To address this, xanthan gum, an anionic rheology modifier, was introduced. We hypothesize that the protonated amino groups ($–NH_3^+$) of chitosan will interact with the ionized carboxyl groups ($–COO^–$) of xanthan gum to form a stable polyelectrolyte complex network. This interaction imparts essential shear-thinning properties required for smooth extrusion and structural retention, making them ideal candidates for fabricating dysphagia-friendly foods.

The predominant forms of nutritional supplements available for cancer patients are either powder or liquid. Patients undergoing clinical treatment frequently ingest liquid nutrition, which can substantially affect their sensory perception, physical condition, and mental state over time. Food 3D printing is an innovative food processing technique that utilizes printing to manipulate raw food products. 3D food printing facilitates the creation of finely formed edibles while permitting individualized modification according to individual dietary and nutritional requirements, thereby enabling precise nutritional customization and addressing health issues stemming from nutritional imbalances.

Currently, it is necessary to develop 3D-printed food that modulates amino acids to impede tumor growth in cancer patients. As a food option for cancer patients, it can enhance their nutritional status and assist in tumor therapy, while also offering a novel eating solution for those with mastication issues, therefore augmenting their quality of life.

2. Materials and methods

2.1. Materials

The −SG diet nutritional powder was designed by Shanghai Wecheer Biotechnology Co., Ltd. (China), which was also used in our previous clinical trial.[5] The amino acid profile consists of essential and non-essential amino acids, excluding only serine and glycine, balanced to meet daily protein requirements (detailed composition in Table S1). The chitosan powder and xanthan gum were provided by Yongxin Food Ingredients Co., Ltd (China). All were food-grade materials.

2.2. Preparation of serine/glycine-free diet formulations

To improve the palatability and clinical applicability of the −SG diet previously used in a phase I clinical trial to enhance immunotherapy efficacy in cancer patients, we developed a 3D-printable formulation using extrusion-based food printing technology. The −SG diet is a fully nutritional formulation specifically designed to restrict serine and glycine intake while maintaining metabolic support. Its protein content is derived entirely from free amino acids (excluding serine and glycine), and it is enriched with dietary fiber, essential vitamins, and minerals to meet comprehensive nutritional needs. For printable adaptation, several trials were conducted to achieve appropriate rheological behavior and sensory properties. The amino acid composition was based on the −SG diet nutritional powder, which incorporated low-protein, plant-based fibers to improve mouthfeel and structural integrity. Xanthan gum was added as a rheological modifier to ensure smooth extrusion and shape retention during printing. This optimized formulation preserved the metabolic efficacy of the original −SG diet while significantly enhancing taste, texture, and overall acceptability for clinical use.

The processing steps for manufacturing the −SG diet-based functional formulation for 3D printing are illustrated in Figure 1. Based on the original recipe, the food matrix (0.5 g) and rheology modifier (0.05 g) were thoroughly mixed with 10 g of freshly prepared water and stirred for 30 min to ensure homogeneity. This mixture (referred to as MIX-1) was subsequently blended in a glass container for an additional five minutes to achieve uniform dispersion. The mixture was stored at 4 °C overnight to allow for complete hydration of the polymer chains and the stabilization of the polyelectrolyte complex network, which is critical for achieving consistent rheological properties and preventing nozzle clogging. Before printing, the −SG diet formulation was equilibrated to room temperature (25 °C), loaded into a syringe, and prepared for extrusion-based 3D food printing.

2.3. 3D printing process

A FOODBOT-S2Pro single-nozzle food 3D printer (Shinnové, China), operating on pneumatic extrusion technology, was employed to fabricate the test samples. The system is equipped with a stainless-steel nozzle with an adjustable diameter range of 0.3–3.0 mm and supports controlled extrusion at temperatures from ambient to 130 °C. Positional accuracy is maintained at 0.1 mm per 100 mm of travel, with a programmable printing speed adjustable between 15 and 70 mm/s. The printer features a 5-inch touchscreen interface with USB-based file transfer and an integrated IoT monitoring module for remote supervision. The overall device dimensions are 420 × 380 × 450 mm, with a maximum printable volume of 150 × 150 × 100 mm.

Unlike conventional hollow cylindrical models commonly used in food printing studies, a solid hexagonal prism geometry was selected in this work. This geometry strictly standardizes the bolus volume and mass distribution for the swallowing assessment, minimizing shape-induced variability, in alignment with methodologies for characterizing texture-modified foods.[19]

2.4. Analytical methods

2.4.1. Response surface optimization

A Box–Behnken design was applied to determine the optimal preparation conditions for the 3D-printed −SG diet.[20] The parameters considered included chitosan powder (1.25–3.75%), xanthan gum (1.25–3.75‰), printing speed (20–30 mm/s), and fill rate (80–100%), as shown in Table 1.

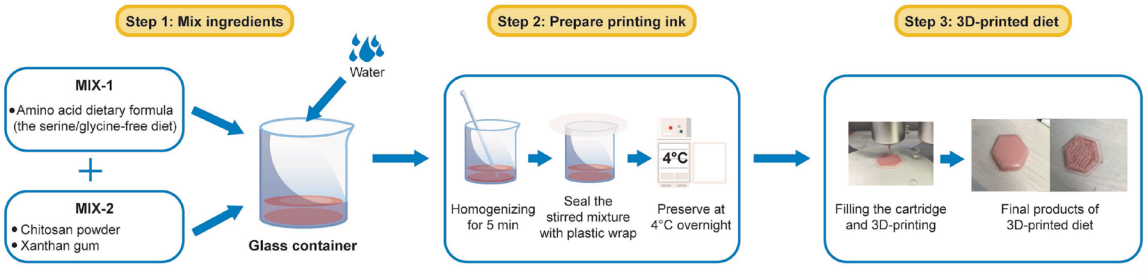

Figure 1. The processing steps from raw materials to the final 3D-printed serine/glycine-free (−SG) diet. Schematic diagrams show the preparation process, including mixing, hydration, and printing. The photographs of the final 3D-printed −SG diet sample show its solid hexagonal prism geometry designed for swallowing assessment.

Table 1. Box–Behnken design

Levels	A: Chitosan powder (%)	B: Xanthan gum (‰)	C: Printing speed (mm/s)	D: Fill rate (%)
–1	1.25	1.25	20	80
0	2.5	2.5	25	90
1	3.75	3.75	30	100

Ink printability was evaluated following our previously established method.[21] Specifically, after photographing the printed samples, the inks were assessed based on four characteristics: layering, filling, edge definition, and overall shape stability. Each characteristic is scored out of 2.5 points, with a maximum total score of 10 points. Inks that are difficult to extrude receive a printability score of 0 points.

The scoring was performed independently by three trained laboratory researchers to ensure inter-rater reliability, and the final score was reported as the mean value. A detailed scoring rubric with visual references is provided in Figure S1.

2.4.2. Textural properties characterization

The texture of the product was determined using a texture analyzer (XTC-18, Shanghai Baosheng Industrial Development Co., Ltd., China). Test parameters were as follows: trigger load of 5 g, pre-test speed of 2.0 mm/s, test speed of 1.0 mm/s, post-test speed of 1.0 mm/s, compression deformation of 10%, and two consecutive cycles.

2.4.3. Fourier transform infrared spectroscopy

The ink powder (2 mg) was mixed with potassium bromide (100 mg) and analyzed using a spectrometer (Bruker alpha II, Bruker Corporation, United States of America [USA]). The scanning range was 400–4000 cm^{-1}, with a resolution of 4 cm^{-1}.

2.4.4. Scanning electron microscope

The ink powder was adhered to the conductive adhesive. The microstructure was observed using a scanning electron microscope (SEM; SUPRA™55, Zeiss, Germany) at an acceleration voltage of 15 kV with a magnification of 500×.

2.4.5. Rheological properties of the optimized formulation

The rheological properties of the optimized food ink formulations containing different edible hydrocolloid concentrations, together with the control sample, were investigated using a dynamic oscillatory rheometer (Kinexus Lab+, Malvern Instruments, United Kingdom). Measurements were carried out using parallel stainless-steel plates with a diameter of 20 mm and a fixed gap of 1 mm. Before testing, the excess sample was carefully trimmed to minimize edge effects. During all measurements, the samples were covered with a rheometer-compatible solvent trap to prevent moisture evaporation.

All rheological tests were conducted at a controlled temperature of 25 °C. Oscillatory frequency sweep measurements were performed within the linear viscoelastic region, which was previously determined, by applying a constant strain of 0.15%. The angular frequency was varied from 0.1 to 50 Hz to evaluate the frequency-dependent viscoelastic behavior of the samples. The storage modulus (G′) and loss modulus (G″) were continuously recorded as a function of frequency to characterize the elastic and viscous responses of the xanthan gum-based formulations.

In addition, the loss tangent ($\tan \delta = G''/G'$) was calculated to assess the relative dominance of viscous and elastic components, while the complex viscosity (η^*) was determined to further describe the structural integrity and deformation resistance of the formulations under oscillatory shear conditions.

2.5. *In vivo* mouse models

A total of 20 female BALB/c mice (6–8 weeks old) were obtained from HFK Bioscience and housed in a specific pathogen-free (SPF) facility under a 12-hour light/dark cycle, with *ad libitum* access to food and water. All experimental procedures were performed under isoflurane anesthesia. Animal experiments were approved by the Ethics Review Committee of Animal Experimentation at Sichuan University. All animal handling and care procedures adhered to the *Guide for the Care and Use of Laboratory Animals* (National Institutes of Health)[22] and complied with the regulations of the Animal Welfare Act. All mice were fed an –SG diet throughout the experiment. The original diet group received a mixture of traditional –SG powder and water at a 1:1 ratio, while the experimental group was administered the 3D-printed –SG diet. All diet

formulations were subjected to food safety analysis prior to use to ensure compliance with nutritional and hygiene standards.

2.6. Measurement of the liver and kidney biochemical indices

All mice fasted overnight before blood collection to minimize metabolic variability. Serum concentrations of liver function (albumin, alanine aminotransferase, aspartate aminotransferase, and total protein) and kidney function (creatinine, uric acid, and blood urea) were measured using a Cobas 8000 modular analyzer (Roche Diagnostics, USA) to evaluate liver and kidney functions.

2.7. Targeted amino acid metabolomics

Organic acid standards were accurately weighed and dissolved in methanol or water to prepare individual stock solutions. Appropriate volumes of each stock were mixed to obtain a combined standard solution, which was then diluted with 30% methanol containing 0.1% formic acid (FA) to prepare working standard solutions at the desired concentrations. All stock and working solutions were stored at 4 °C before use. For sample preparation, an appropriate amount of the sample was placed into a 2 mL centrifuge tube, and 500 μL of 30% methanol aqueous solution (0.1% FA) was added. The mixture was vortexed for 60 seconds, followed by the addition of two stainless steel grinding beads. The tube was then subjected to tissue grinding at 55 Hz for 1 min, and this process was repeated at least twice to ensure thorough homogenization. After grinding, samples were centrifuged at 12,000 rpm for 10 min at 4 °C. The supernatant was collected and diluted fivefold with 30% methanol aqueous solution (0.1% FA), vortexed for 30 s, and filtered through a 0.22 μm membrane. The final filtrate was transferred into a high-performance liquid chromatography vial for subsequent analysis.

2.8. Sensory assessment

A sensory evaluation was conducted to investigate the impact of 3D-printed food on the palatability and overall acceptability of −SG diet. Twenty healthy volunteers (aged 22–50, with no history of dysphagia or taste disorders) were enrolled after providing informed consent. The protocol was approved by the Ethics Committee of West China Hospital, Sichuan University, and the study was registered with the Chinese Clinical Trial Registry (Registration number: ChiCTR2300067929). Healthy volunteers were included to enable objective evaluation of baseline sensory properties (texture, flavor, appearance) without the confounding effects of chemotherapy-induced dysgeusia. Sensory assessments were carried out in individual booths under controlled environmental conditions. Each sample, including both the unprinted and printed versions of the formulation, was labeled with a random three-digit code and presented in a balanced and sequential manner (Table S2). Panelists evaluated four attributes—appearance, texture, flavor, and smell—using a structured 10-point scoring system with defined criteria. Appearance was assessed based on shape regularity, texture on firmness and surface structure, flavor on saltiness and strawberry notes without undesirable aftertastes, and smell on the intensity of strawberry aroma. Each attribute had a maximum of 10 points, yielding a total possible score of 40, which represented overall acceptability. All evaluations were performed in triplicate across different days to ensure consistency and reliability.

2.9. Direct swallowing test for 3D-printed serine/glycine-free diet

To assess the clinical acceptability and swallowing safety of −SG diet, a direct swallowing test was conducted among another twenty cancer patients who were recruited with informed consent under approval from the Ethics Committee of Sichuan University.[23,24] The test aimed to compare the swallowing performance of the conventional liquid formulation with that of the 3D-printed version, which featured a semi-solid texture designed to reduce discomfort during ingestion (Table S3). Detailed demographic information (including cancer type and stage) is provided in Table S4. This self-controlled (paired) design, in which each patient underwent both the control (liquid) and intervention (3D-printed) tests, minimizes the impact of inter-subject heterogeneity (e.g., variations in age or disease stage) on the comparative outcomes. Each participant underwent two sequential subtests. The first involved the 3D-printed diet, where patients were given an initial portion of one-third to one-half teaspoon, followed by five additional half-teaspoon servings. The second subtest involved the conventional liquid formulation, with patients instructed to consume 50 mL as quickly as possible. Trained investigators closely monitored patients after each administration and immediately terminated the test if any of the predefined signs of aspiration occurred. These included failed or delayed swallowing, involuntary coughing, drooling, or a noticeable change in voice quality. Each of the four indicators was scored according to a structured system: swallowing was rated from zero (not possible) to two (successful), while coughing, drooling, and voice change were each scored zero if present and one if absent. A cumulative score was calculated to quantify the overall swallowing performance. This evaluation provided clinically relevant evidence that the 3D printing formulation improved texture-related swallowing tolerance in cancer patients compared to the original liquid version.

2.10. Statistical analysis

All data are presented as mean values with standard error of the mean, based on three independent replicates unless otherwise stated. Statistical analyses were performed using GraphPad Prism 8 software (GraphPad Software Inc., USA). One-way analysis of variance (ANOVA) was conducted to evaluate differences among groups, followed by Tukey's multiple comparison test for post hoc analysis. For both sensory evaluation and direct swallowing tests, which followed a self-controlled (paired) design, both unpaired t-tests and paired *t*-tests were performed to provide a comprehensive comparison between the original and 3D-printed diets. Specifically, the paired t-test was used to account for individual-specific improvements, while the unpaired t-test assessed the general difference between the two formulation types. A *p*-value less than 0.05 was considered statistically significant. Statistical significance is indicated as follows: $^{*}p < 0.05$; $^{**}p < 0.01$; $^{***}p < 0.001$; $^{****}p < 0.0001$. Unless otherwise specified, asterisks denote comparisons with the control group.

3. Results

3.1. Optimization of 3D-printed serine/glycine-free diet

Table 2 showed the response surface results for the 3D-printed −SG diet. Multivariate regression analysis was performed on the data generated from the BBD experiment using Design-Expert 13 (Stat-Ease Inc., USA). The quadratic polynomial equation between the 3D-printed −SG diet score and the variables was:

$$Y(Score) = 7.07 - 2.24A - 1.20B - 1.03C + 0.40D + 0.13AB - 0.46AC + 0.30AD + 0.00BC - 0.88BD + 0.29CD - 0.80A^2 - 0.65B^2 - 0.86C^2 - 0.59D^2 \quad (1)$$

It is worth noting that higher variability was observed in the printability scores of certain non-optimal formulations, such as running with extreme chitosan/xanthan gum ratios. This variation reflects the inherent instability of the ink during extrusion; formulations lacking optimal viscoelasticity tended to exhibit inconsistent structural deposition across replicates, whereas the optimized formulation (Ink10) demonstrated high reproducibility.

Additionally, the significance of the regression model was tested using ANOVA, with *F*-values and *p*-values calculated. As shown in Table 3, the model was statistically significant ($F = 5.58$, $p < 0.05$), whereas the lack-of-fit test was not statistically significant ($F = 1.74$, $p > 0.05$), indicating that the model has good applicability in predicting and analyzing the 3D-printed −SG diet. The model's coefficient of determination ($R^2 = 0.8480$), coefficient of variation of 19.83%, and adequacy of precision (Adeq precision) of 8.9518—which far exceeds the critical value of 4—validate the reliability of the experimental results.[20,25]

Figure 2A–F illustrates the interaction effects of any two factors on the 3D-printed −SG diet score. The contour lines in each interaction plot form elliptical shapes, indicating the presence of interactions between any two factors. Steeper slopes correspond to more pronounced interactions. Based on response surface analysis results, the optimal preparation parameters for 3D-printed −SG diet were: chitosan powder 1.25%, xanthan gum 1.28‰, printing speed 24.41 mm/s, fill rate 98.78%. Under these conditions, the theoretical score reached 9.52. For practicality, the validation experiments were conducted at chitosan powder 1.25%, xanthan gum 1.25‰, printing speed 25 mm/s, and fill rate 100%. Three experiments yielded an actual score of 9.63 ± 0.12. The minimal deviation between actual and theoretical values demonstrates the model's accurate representation of the optimization process.[26]

3.2. Effects of 3D printing formulation on the quality characteristics of 3D-printed products

To comprehensively elucidate the structure–function relationships during the printing process, we further expanded the formulation design to include a broader range of samples (designated as Ink1–11), covering both the compositions within and outside the initial response surface design. Detailed compositions and design logic for these formulations are summarized in Table S7.

Specifically, Ink1, Ink10, and Ink9 were designed to evaluate the synergistic effects of varying both chitosan and xanthan gum at a fixed ratio while maintaining constant printing speed and fill rate. To isolate the impact of individual components, Ink4, Ink7, and Ink10 were used to compare variations in chitosan concentration, while Ink5, Ink8, and Ink10 focused on the effects of xanthan gum concentration, with all other parameters held constant. Furthermore, the influences of processing parameters were investigated by comparing Ink2, Ink10, and Ink11 for different fill rates, and Ink3, Ink6, and Ink10 for varying printing speeds.

To elucidate the structure-function relationships underlying the optimization process, three representative formulations from the experimental design were selected for detailed characterization: Ink5 (high xanthan gum ratio), Ink9 (high chitosan ratio), and Ink10 (optimized center point). These samples cover the range of rheological behaviors observed across the 29 experimental runs. Texture is a critical determinant of swallowing safety and patient acceptance in foods for special medical purposes, particularly for cancer patients who require

Table 2. Response surface design rating for printing formulas.

Code	A: Chitosan powder (%)	B: Xanthan gum (‰)	C: Printing speed (mm/s)	D: Fill rate (%)	Score
1	2.5	3.75	30	90	2.33 ± 0.62
2	1.25	3.75	25	90	7.33 ± 1.03
3	2.5	1.25	25	80	6.00 ± 1.41
4	2.5	1.25	30	90	5.67 ± 0.47
5	2.5	1.25	25	100	9.50 ± 0.00
6	2.5	3.75	25	80	4.00 ± 1.22
7	2.5	2.5	30	100	4.33 ± 0.94
8	2.5	3.75	20	90	5.33 ± 0.24
9	2.5	2.5	25	90	7.83 ± 1.03
10	2.5	2.5	25	90	8.17 ± 1.18
11	1.25	2.5	30	90	8.17 ± 0.62
12	2.5	2.5	20	100	6.50 ± 0.71
13	3.75	2.5	30	90	2.33 ± 0.85
14	3.75	2.5	25	80	2.33 ± 0.24
15	2.5	2.5	20	80	7.50 ± 0.41
16	2.5	2.5	30	80	4.17 ± 1.03
17	2.5	2.5	25	90	5.83 ± 1.18
18	3.75	1.25	25	90	3.67 ± 0.85
19	2.5	2.5	25	90	6.83 ± 0.24
20	2.5	3.75	25	100	4.00 ± 0.41
21	3.75	2.5	20	90	3.67 ± 0.94
22	2.5	2.5	25	90	6.67 ± 0.85
23	1.25	2.5	25	100	8.17 ± 1.03
24	1.25	1.25	25	90	7.67 ± 0.24
25	1.25	2.5	25	80	7.83 ± 0.24
26	3.75	2.5	25	100	4.17 ± 1.03
27	1.25	2.5	20	90	7.67 ± 0.47
28	2.5	1.25	20	90	8.67 ± 0.47
29	3.75	3.75	25	90	3.83 ± 0.62

Note: Data are presented as mean ± standard deviation (n = 3 independent replicates per formulation.

long-term consumption of –SG diet. As shown in Figure 3A, comparative texture profile analysis revealed that the optimized formulation (Ink10) exhibited the most balanced textural profile, characterized by the concurrent enhancement of stiffness, elasticity, and chewiness. In contrast, formulations with higher xanthan gum content (Ink5 and Ink9) showed a clear deterioration in texture quality. Excessive system viscosity led to abnormally elevated adhesiveness, which in turn constrained the effective development of stiffness and elastic responses. Further increasing the chitosan powder content (Ink9) failed to compensate for these deficiencies and instead intensified the decline in cohesiveness and chewiness, indicating that the influence of hydrocolloid–powder incorporation on texture is not linearly additive but governed by compositional synergy. This excessively

Table 3. ANOVA for the regression model

Source	Sum of squares	df	Square	*F*-value	*p*-value	Significant (Yes/No)
Model	105.78	14	7.56	5.58	0.0014	Yes
A: Chitosan powder	60.03	1	60.03	44.34	<0.0001	
B: Xanthan gum	17.18	1	17.18	12.69	0.0031	
C: Printing speed	12.69	1	12.69	9.37	0.0085	
D: Fill rate	1.95	1	1.95	1.44	0.2497	
AB	0.0625	1	0.0625	0.0462	0.8330	
AC	0.8464	1	0.8464	0.6252	0.4423	
AD	0.5625	1	0.5625	0.4155	0.5296	
BC	0.0000	1	0.0000	0.0000	1.0000	
BD	3.06	1	3.06	2.26	0.1548	
CD	0.3364	1	0.3364	0.2485	0.6259	
A^2	4.11	1	4.11	3.04	0.1032	
B^2	2.75	1	2.75	2.03	0.1759	
C^2	4.78	1	4.78	3.53	0.0811	
D^2	2.25	1	2.25	1.66	0.2183	
Residual	18.95	14	1.35			
Lack of Fit	15.41	10	1.54	1.74	0.3125	No
Pure Error	3.54	4	0.8857			
Cor total	124.73	28				
R^2 = 0.8480				C.V. = 19.83		AP = 8.9518

Abbreviations: AP: Adeq Precision (measures the signal to noise ratio); Cor total: Corrected Total; CV: Coefficient of variation.

high yield stress directly correlates with the undesirable hardness and adhesiveness observed in the texture profile analysis for Ink9, confirming that while a strong network is needed for shape fidelity, excessive rigidity compromises the semi-solid texture required for dysphagia diets.

Figure 3B presents the Fourier transform infrared (FTIR) spectra of the three formulations, which exhibit highly similar characteristic absorption bands, indicating that no new covalent bonds were formed during formulation or printing. Notably, differences in absorption intensity and slight peak shifts were observed, suggesting that variations in chitosan powder and xanthan gum contents modulated intermolecular interactions rather than chemical bonding. All samples display a broad absorption band in the range of approximately 3200–3400 cm^{-1}, which is attributed to the stretching vibrations of O–H and N–H groups, primarily originating from polysaccharides, amino acid residues, and residual moisture. Ink10 shows a moderate absorption intensity with a relatively smooth band profile, which may suggest a stable intermolecular interaction supported by the rheological evidence. Consistent with this observation, its uniformly porous microstructure (Figure 3C) facilitates more stable infrared absorption and scattering.

In contrast, Ink5 exhibits a broader and more intense absorption band in this region. The higher xanthan gum content introduces an increased density of hydroxyl (–OH) groups, which likely restricts molecular mobility and enhances system adhesiveness. Moreover, the denser microstructure intensifies infrared scattering, resulting in reduced transmittance. This interaction state is in good agreement with SEM observations, which reveal a compact and irregular morphology characterized by poorly defined pores and partial structural collapse, implying limited stress relaxation and constrained structural rearrangement during printing. Ink9, containing a higher chitosan powder content, consistently shows lower transmittance across the entire spectral range, particularly within the 3600–3000 cm^{-1} and 1200–800 cm^{-1} regions. The

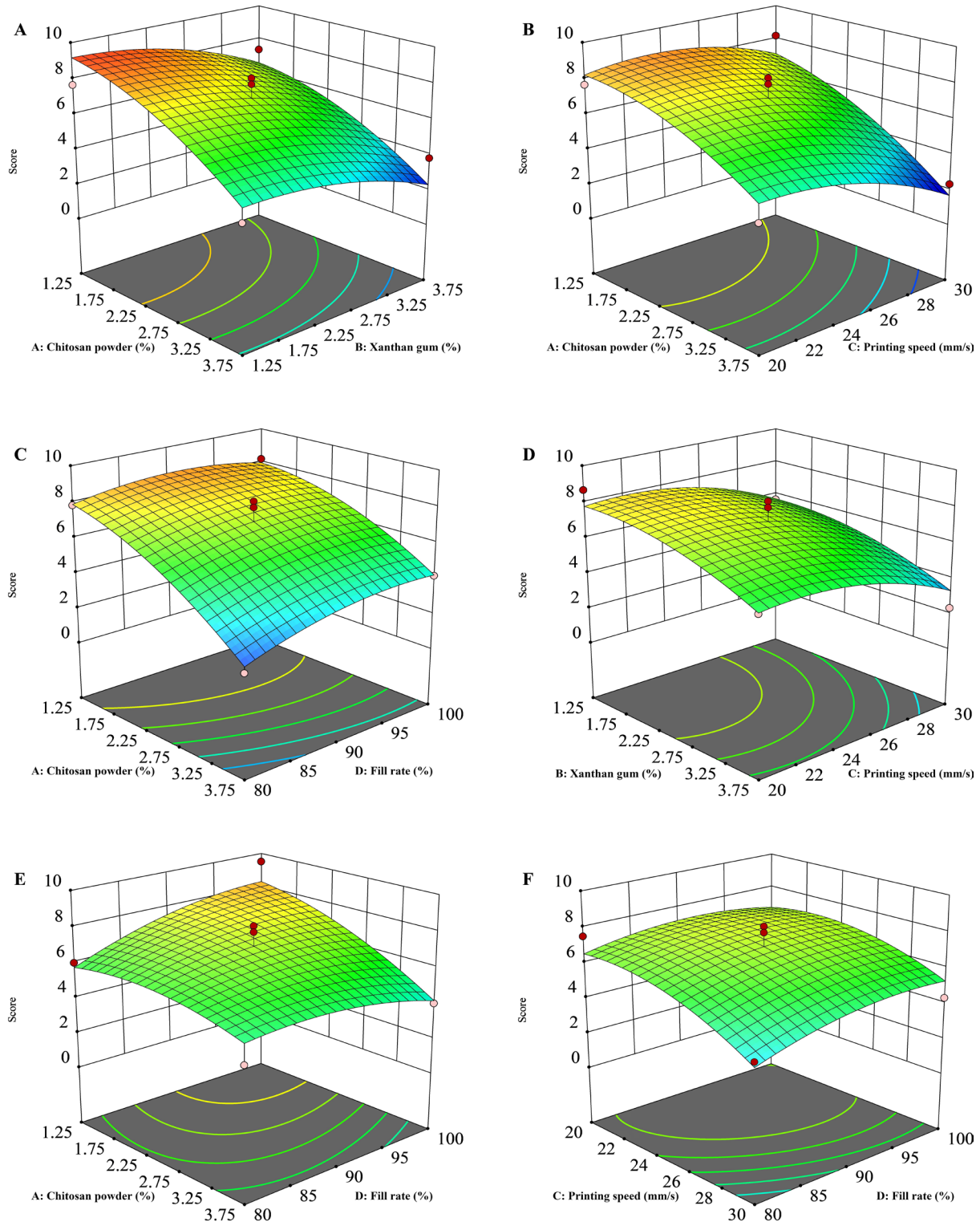

Figure 2. The 3D surface plots showing interactions of any two variables on the 3D-printed –SG diet score. (A) Interaction between chitosan powder and xanthan gum. (B) Interaction between chitosan powder and printing speed. (C) Interaction between chitosan powder and fill rate. (D) Interaction between xanthan gum and printing speed. (E) Interaction between xanthan gum and fill rate. (F) Interaction between printing speed and fill rate.

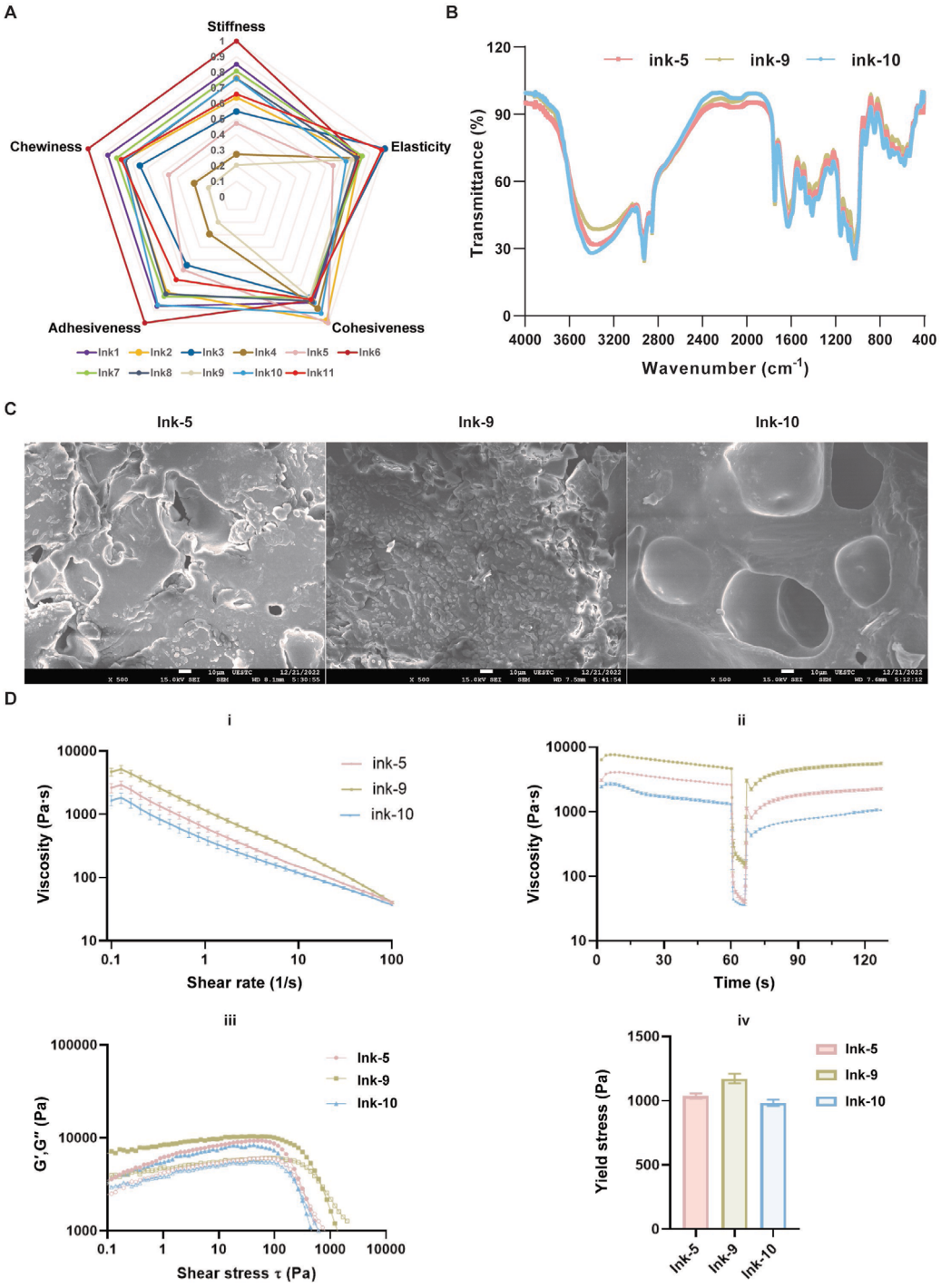

Figure 3. The characteristics of the optimized 3D-printed −SG diet. (A) Texture profile analysis of different ink formulations, showing hardness, elasticity, chewiness, and adhesiveness. (B) Fourier transform infrared spectra of three representative ink formulations (Ink5, Ink9, Ink10). (C) Scanning electron microscopic images of the microstructure of the inks (Scale bar: 10 μm; magnification: 500×). (D) Rheological properties: (i) Viscosity vs. shear rate, (ii) Storage modulus (G′) and loss modulus (G″) vs. strain, (iii) Thixotropic behavior, (iv) Yield stress.

increased absorbance can be directly attributed to the elevated concentration of chitosan, which introduces additional hydroxyl (O–H) groups and glycosidic (C–O–C) linkages, thereby enhancing vibrational absorption. Correspondingly, SEM images reveal a disordered pore morphology and pronounced structural heterogeneity in Ink9, indicating that although local intermolecular interactions are strengthened, excessive solid loading leads to uneven stress distribution and compromises overall structural continuity.

To elucidate the rheological origins of these textural differences, small-amplitude oscillatory shear and steady-flow measurements were conducted on Ink5, Ink9, and Ink10. All three inks exhibited pronounced shear-thinning behavior (Figure 3Di). At low shear rates, extensive molecular entanglement generated dense network structures, maintaining viscosities on the order of 10^3–10^4 Pa·s and thereby ensuring structural stability before printing. Upon increasing the shear rate to 100 s^{-1}, network disentanglement caused a sharp viscosity reduction to approximately 10 Pa·s, satisfying the flow requirements for extrusion. Notably, Ink9 displayed a substantially higher low-shear viscosity than Ink5 and Ink10, whereas their viscosities converged under high shear, consistent with concentration-dominated effects in chitosan powder–xanthan gum composite systems. Dynamic rheological analysis (Figure 3Dii) further demonstrated that all inks behaved as elastic-dominated, solid-like materials ($G' > G''$) in the low-strain regime, a prerequisite for 3D-printed shape fidelity. Beyond a critical stress threshold, both moduli decreased synchronously, marking an elastic-to-viscous transition that enabled flow. Ink9 exhibited the highest G' values at low strain, reflecting enhanced network rigidity imparted by higher polymer concentration. Yield stress measurements (Figure 3Div) corroborated these findings, showing that Ink9 required significantly greater external force to disrupt its internal structure. While such high yield stress favors the construction of complex geometries, it may simultaneously increase extrusion resistance, necessitating the use of larger nozzle diameters to avoid clogging. Time-dependent viscosity measurements (Figure 3Diii) revealed typical thixotropic behavior for all inks, characterized by rapid viscosity breakdown under shear followed by gradual structural recovery upon shear removal. Ink9 exhibited the largest hysteresis loop area, indicating accelerated network dissociation and re-entanglement associated with high polymer loading. This rheological feature supports the dual printing requirement of smooth extrusion and rapid shape stabilization after deposition. Taken together, the combined texture and rheological analyses identify Ink10 as achieving the most favorable balance between structural stability, printability, and oral sensory performance, providing a rational formulation strategy for the design of 3D-printed foods tailored to –SG dietary applications.

3.3. *In vivo* safety assessment and metabolic modulation

To assess the biocompatibility and metabolic efficacy of the 3D-printed diet, a comparative *in vivo* study was conducted using BALB/c mice. As illustrated in Figure 4A and 4B, mice in the experimental group (fed the 3D-printed –SG diet) exhibited normal activity and feeding behavior throughout the intervention period, similar to those in the control group (fed the original –SG diet).

Figure 4C and 4D shows body-weight changes over time in both groups. The final body weights at the end of the intervention were comparable between the two groups (Figure 4C). The mice receiving the 3D-printed –SG diet maintained stable body weight throughout the study, with no significant differences compared to the control group fed the original –SG diet (Figure 4D). The results indicated that the printed formulation provided adequate energy without inducing malnutrition or cachexia.

Physiological safety was further evaluated by measuring key biochemical indices using the Cobas® 8000 modular analyzer (Roche Diagnostics, USA) after the intervention (Figure 4E). All liver function markers (albumin, alanine aminotransferase, aspartate aminotransferase, total protein) and kidney function (creatinine, uric acid, blood urea) remained within normal ranges. No statistically significant differences were observed between the original diet group and the 3D-printed diet group. These results confirm that incorporation of chitosan and xanthan gum, as well as the 3D printing process, did not introduce systemic toxicity.

Most importantly, targeted metabolomics analysis was performed to assess whether the 3D-printed diet preserved the intended metabolic restriction of serine and glycine. As shown in Figure 4F–H**,** serum concentrations of both serine and glycine were significantly lower in mice fed the 3D-printed –SG diet compared to the levels of other amino acids, and were also reduced to a similar extent as observed in the control group fed the original –SG diet. This confirms that the 3D-printed formulation preserves the functional "metabolic starvation" effect of the original powder. These findings demonstrate that the 3D-printed –SG diet is biologically safe, nutritionally adequate, and metabolically active, providing a solid foundation for its potential use in clinical nutrition support for cancer patients.

3.4. Sensory evaluation

Sensory evaluation scores are presented in Figure 5A

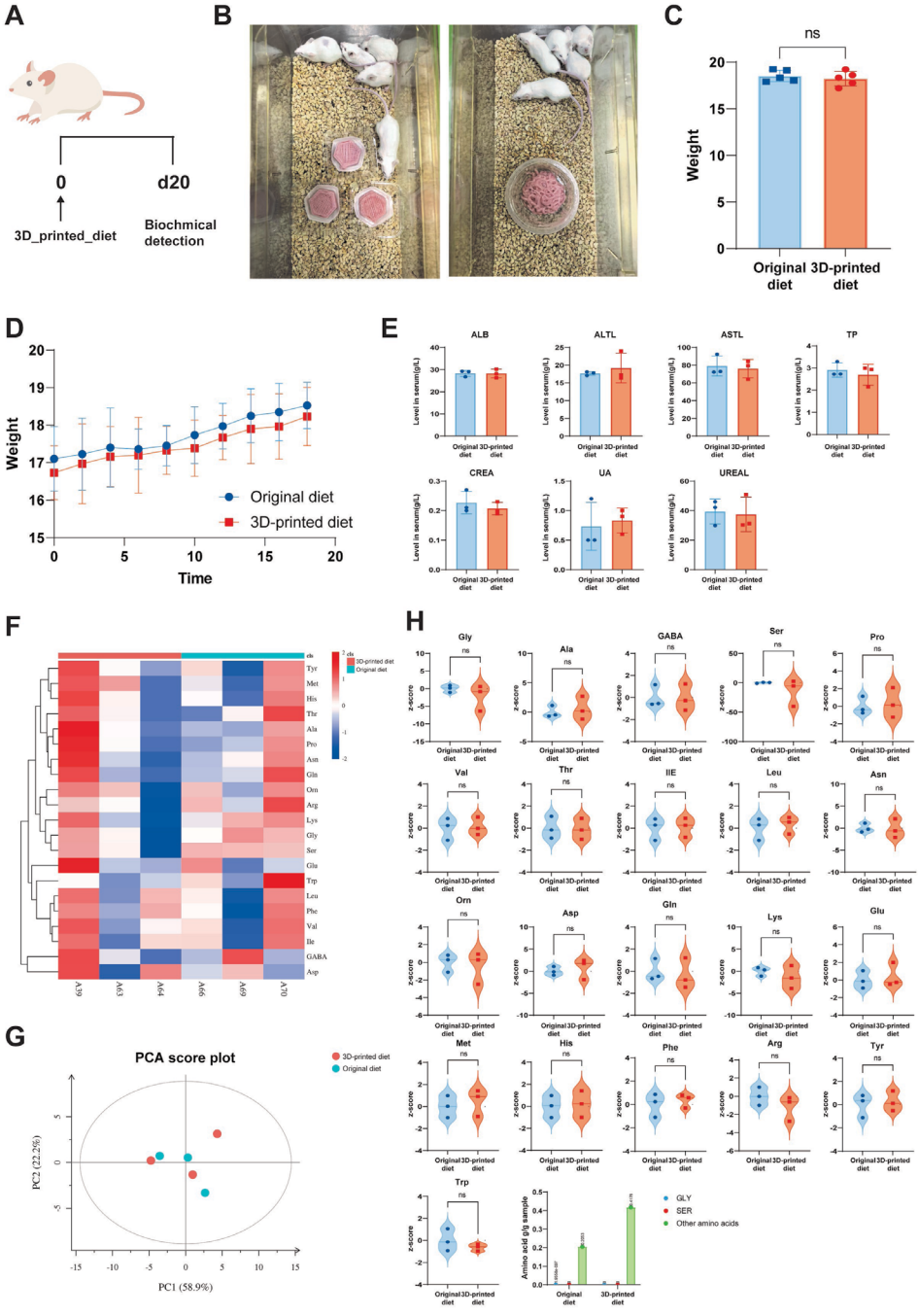

Figure 4. *In vivo* evaluation of biological safety and serum amino acid modulation by the 3D-printed serine/glycine-free (–SG) diet. (A) Experimental timeline (day 0 to day 20). (B) Representative images showing feeding behavior in mice receiving the original –SG diet (right) or the 3D-printed diet (left) (*ad libitum*). Although the diets differ in physical appearance owing to texture (solid blocks vs. paste/liquid), body-weight monitoring (D) indicated comparable overall intake between groups. (C) Final body weight comparison. (D) Body weight changes over time. (E) Serum biochemical indices of liver and kidney functions: albumin (ALB), alanine aminotransferase (ALTL), aspartate aminotransferase (ASTL), total protein (TP), creatinine (CREA), uric acid (UA), and blood urea (UREAL). (F–H) Serum amino acid profiles in mice fed the original –SG diet (control) or the 3D-printed –SG diet, including serine (Ser), glycine (Gly), and other quantified amino acids (gamma-aminobutyric acid [GABA], alanine [Ala], valine [Val], leucine [Leu], isoleucine [Ile], proline [Pro], phenylalanine [Phe], tryptophan [Trp], methionine [Met], threonine [Thr], aspartate [Asp], asparagine [Asn], glutamate [Glu], glutamine [Gln], lysine [Lys], histidine [His], arginine [Arg], tyrosine [Tyr], and cysteine [Cys]).

and Table S5. This sensory analysis provided quantitative evidence that 3D printing significantly improved the sensory quality and clinical usability of the −SG dietary formulation. The appearance, texture, flavor, smell, and overall acceptability scores for the original diet were 6.53 ± 0.74, 6.95 ± 0.65, 7.26 ± 0.85, 6.88 ± 0.80, and 27.63 ± 1.59, respectively, indicating an overall rating between "like slightly" and "like moderately." The 1.25‰ xanthan gum-added sample received significantly higher scores than the original diet for appearance, texture, flavor, smell, and overall acceptability ($p < 0.05$), with corresponding values of 8.12 ± 0.83, 8.07 ± 0.93, 8.12 ± 0.84, 8.05 ± 0.63, and 32.35 ± 1.69, respectively. Clinically, this shift represents a transition from a "tolerable" diet (scores ~6–7) to a "highly palatable" diet (scores >8). Such an improvement is critical for ensuring long-term patient compliance, as taste fatigue is a primary cause of malnutrition in oncology patients on restricted diets. The unexpectedly higher flavor scores for the 3D-printed diet can be attributed to the taste-masking effect of the hydrocolloid matrix. Free amino acids in the original liquid diet often impart a bitter or metallic aftertaste. The formation of a polyelectrolyte complex network likely entraps these amino acids, reducing their immediate direct contact with taste buds, while effectively retaining the added strawberry aroma for a more sustained and pleasant flavor release. The consistently higher scores for the xanthan gum-added samples could be attributed to the pseudoplastic behavior and network formation facilitated by xanthan gum. Similarly, Liu *et al.*[27] reported that as the amount of xanthan gum added to 3D-printed egg white protein-based products increased, the products received higher sensory scores due to the contribution of

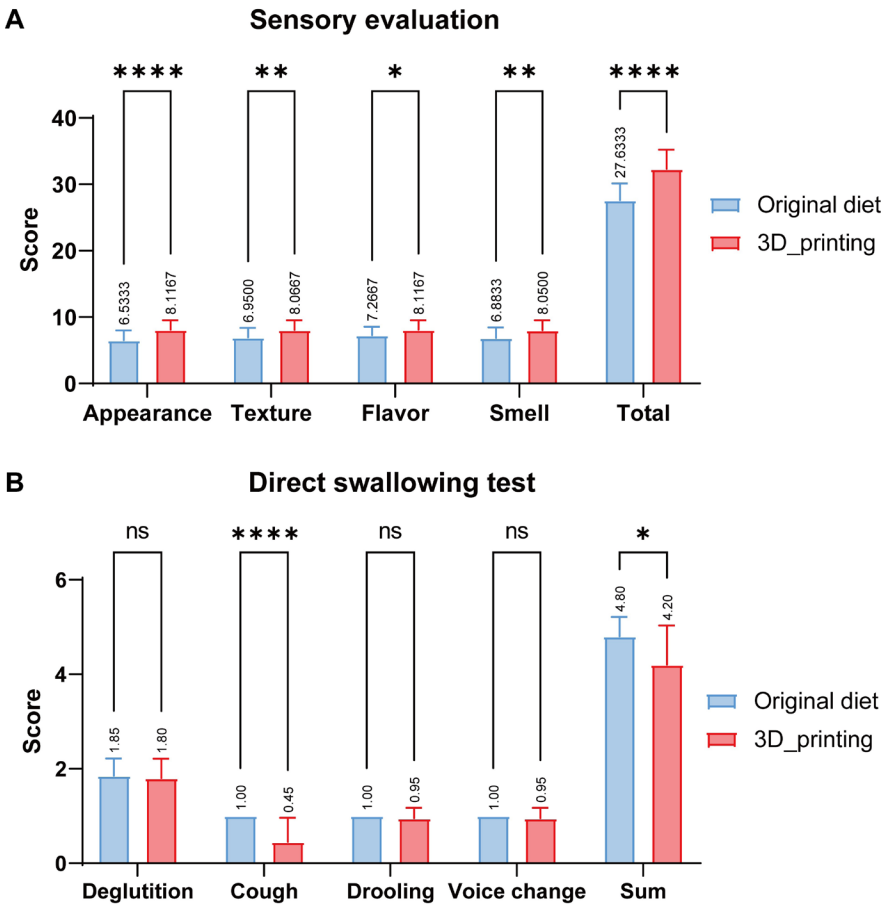

Figure 5. Sensory evaluation and direct swallowing test. (A) Sensory scores for appearance, texture, flavor, smell, and overall acceptability of original vs. 3D-printed serine/glycine-free diet. (B) Direct swallowing test results, including deglutition score, involuntary coughing, drooling, voice change, and total swallowing performance score.
Notes: ns: Not significant; *$p < 0.05$; **$p < 0.01$; ***$p < 0.001$; ****$p < 0.0001$.

xanthan gum addition to their rheological properties.

3.5. Direct swallowing test for 3D-printed serine/glycine-free diet

A direct swallowing assessment was conducted in twenty cancer patients to compare the swallowing safety of the original liquid formulation with that of the 3D-printed −SG diet (Figure 5B and Table S6). As shown in Figure 5B and Table S6, no significant difference was observed in the deglutition score between the two diets (1.80 ± 0.41 vs. 1.85 ± 0.37, $p = 0.6867$). Notably, while the basic mechanical ability to swallow (deglutition score) remained similar between groups (indicating both forms could be ingested), the semi-solid texture markedly reduced adverse safety events, specifically involuntary coughing (0.45 ± 0.51 vs. 1.00 ± 0.00, $p < 0.0001$). This dissociation highlights that the 3D-printed diet improves safety by preventing premature bolus spillage into the airway without compromising the ease of bolus transport. Consequently, the total swallowing performance score was significantly higher for the 3D-printed diet compared with the original formulation (4.8 ± 0.41 vs. 4.2 ± 0.83, $p = 0.0064$ by unpaired *t*-test; $p = 0.0003$ by paired *t*-test). These findings indicate that the semi-solid texture generated via 3D printing effectively improves swallowing tolerance and reduces aspiration-related symptoms in cancer patients.

4. Discussion

This study demonstrates the successful development and clinical evaluation of a 3D-printed −SG diet aimed at improving the sensory properties and clinical usability of amino acid-modified nutrition therapy in cancer patients. Serine and glycine are non-essential amino acids that play critical roles in tumor metabolism and immune evasion, and previous studies have shown that dietary restriction of these amino acids can enhance the efficacy of immunotherapies by modulating the tumor microenvironment.[5] However, the clinical application of the −SG diet has been limited by poor palatability, leading to reduced patient compliance and treatment adherence.[28]

By applying extrusion-based 3D food printing technology, we reformulated the SG-free diet into a semi-solid, visually appealing product with improved structural integrity and sensory qualities. Amino acid profiling confirmed that the 3D printing process did not compromise the intended amino acid composition, preserving the therapeutic restriction of serine and glycine. *In vivo* experiments in mice verified the safety of the 3D-printed formulation, with no adverse effects on body weight or key organ functions, and the expected reduction in circulating serine and glycine levels was observed, aligning with previous metabolic studies.[5]

From a material science perspective, the success of this formulation is attributed to the electrostatic interaction between the matrix components. As indicated by our FTIR and rheological data, the positively charged amino groups of chitosan interact with the negatively charged carboxyl groups of xanthan gum to form a stable polyelectrolyte complex. This intermolecular network significantly enhances the zero-shear viscosity and yield stress of the ink, addressing the common issue of structural collapse in extrusion-based printing.[29] Importantly, this physical cross-linking avoids the need for chemical cross-linkers, ensuring the high biosafety observed in our animal models.

The rheological mechanism underlying the improved swallowing safety lies in the specific flow behavior of the chitosan-xanthan gum complex. The 3D-printed diet exhibits pseudoplasticity (shear-thinning), meaning its viscosity decreases under the shear stress of swallowing, facilitating bolus transport, yet recovers quickly to prevent premature flow into the airway (aspiration). This aligns with the requirements for texture-modified diets (Level 4/5) recommended for dysphagia management by the International Dysphagia Diet Standardisation Initiative for dysphagia management.[30] Unlike liquid formulations, which travel too quickly for the epiglottic closure reflex in some patients, the printed semi-solid structure provides adequate mechanical stimulation to trigger the swallowing reflex while maintaining cohesiveness to prevent bolus fragmentation, directly explaining the significant reduction in coughing events observed in our study. These results corroborate emerging evidence that 3D printing can precisely tailor food texture to enhance swallowing safety in high-risk populations.[31]

Most notably, both the sensory evaluation and direct swallowing test provided compelling evidence for improved clinical acceptability. Compared to the traditional powdered or liquid formulation, the 3D-printed −SG diet received significantly higher scores in appearance, texture, flavor, and smell, and was associated with fewer incidents of coughing or discomfort during swallowing. These findings are consistent with prior work indicating that improved rheological properties—such as those achieved with xanthan gum incorporation—can enhance the sensory experience of 3D-printed therapeutic foods.[27] Our study extends this evidence to a clinical context involving cancer patients, offering a practical solution to the long-standing issue of nutritional adherence in medically restricted diets. The direct swallowing test revealed that the 3D-printed diet was better tolerated in patients, with a statistically significant reduction in involuntary coughing and higher

overall swallowing performance. This suggests that beyond taste and visual appeal, the mechanical texture and ease of consumption are critical parameters for successful integration of therapeutic diets into oncology care.

Despite the promising findings, several limitations in this study must be acknowledged. First, regarding study design and population: The clinical evaluation was conducted with a relatively small sample size (n = 20). Although the self-controlled (paired) design minimized the impact of inter-patient heterogeneity (e.g., age, tumor stage), larger multi-center trials are needed to confirm the generalizability of these findings across diverse cancer populations. Second, regarding methodology: The administration protocols in the swallowing test (teaspoon feeding for semi-solids vs. 50 mL bolus drinking for liquids) were distinct. While designed to mimic realistic consumption patterns, this difference introduces a potential confounding variable, as the slower ingestion rate of the 3D-printed diet may have contributed partially to the observed reduction in coughing events independent of texture. Third, regarding long-term feasibility: This study only assessed immediate sensory acceptance. Whether patients can maintain long-term adherence to the hexagonal-prism geometry without experiencing "shape fatigue" or flavor monotony remains unknown and requires longitudinal investigation. Fourth, regarding scalability: The practical implementation of 3D printing in a busy hospital kitchen faces significant hurdles. The current single-nozzle printing speed and the operational time required for ink preparation and equipment cleaning may limit throughput. Future work must focus on developing multi-nozzle systems or pre-packaged industrial solutions to improve the cost-effectiveness and efficiency of deployment. Finally, regarding therapeutic implications: While our *in vivo* data confirmed that the 3D-printed diet successfully depletes serum serine and glycine, the logical step from "metabolic depletion" to "enhanced immunotherapy efficacy" represents a theoretical hypothesis based on preclinical literature. This study validates the functional delivery vehicle; however, its actual synergistic effect with immunotherapy in human patients remains to be verified in rigorous future oncological trials.

Taken together, our findings demonstrate that 3D food printing provides a feasible strategy to overcome sensory and compliance barriers in the clinical implementation of amino acid-modified diets. This technology not only retains nutritional and therapeutic integrity but also aligns with the principles of personalized nutrition, allowing for individual adaptation in terms of taste, texture, and portioning. Future research should also investigate advanced printing strategies to further enhance product quality. For instance, Tian *et al.*[32] demonstrated that optimizing nozzle geometry and multimaterial switching can significantly improve printing fidelity and structural resolution. Furthermore, Maldonado-Rosas *et al.*[33] highlighted the role of controlled void shapes in tailoring the mechanical properties of printed foods. Incorporating such internal structural designs could allow for even more precise control over the texture and breakdown mechanics of dysphagia diets in the future.

5. Conclusion

This study successfully developed a 3D-printed −SG functional food using a chitosan-xanthan gum polyelectrolyte complex matrix. Through optimization, a formulation containing 1.25% chitosan and 1.25‰ xanthan gum was identified, exhibiting superior printability and structural fidelity. Crucially, the conversion of the delivery modality from liquid to semi-solid significantly mitigated clinical adverse reactions, evidenced by a 55% reduction in involuntary coughing events and a 17.1% improvement in sensory acceptability compared to conventional liquid controls. Furthermore, *in vivo* evaluations verified that this physicochemical reconstruction preserved the biological safety and the targeted metabolic depletion of serine and glycine. Collectively, these findings validate 3D food printing as a vital technological solution to resolve swallowing barriers, thereby enhancing patient adherence to metabolic interventions in oncology care.

Acknowledgments

We would like to express our sincere gratitude to all the patients and volunteers who participated in the sensory evaluation and direct swallowing tests; their cooperation was essential to the clinical validation of this study. We also thank Shanghai Wecheer Biotechnology Co., Ltd. (Shanghai, China) for designing the original −SG diet nutritional powder and Yongxin Food Ingredients Co., Ltd. (Guangzhou, China) for providing the food-grade chitosan and xanthan gum. We appreciate the technical support provided by the State Key Laboratory of Biotherapy (West China Hospital) and the School of Integrated Circuit Science and Engineering (UESTC) for assisting with the material characterization experiments (SEM and Rheology).

Funding

The authors declare that no funds, grants, or other financial support were received during the preparation of

this manuscript.

Conflict of interest

Yi Zhang serves as the Editorial Board Member of the journal, but did not in any way involve in the editorial and peer-review process conducted for this paper, directly or indirectly. Other authors declare they have no competing interests.

Author Contributions

Conceptualization: Xuelei Ma, Yi Zhang, Xiaosheng Zhang
Data Curation: Yuhao Wei, Yuanyuan Chen
Formal analysis: Yuhao Wei, Yuanyuan Chen
Investigation: Yuhao Wei, Yuanyuan Chen, Guangqi Li, Yu Xiang, Jiangfei Li
Methodology: Yuhao Wei, Yuanyuan Chen, Guangqi Li
Project administration: Xuelei Ma
Resources: Xuelei Ma, Yi Zhang, Yi-Ping Ho, Juan Huang
Supervision: Xuelei Ma, Yi Zhang, Xiaosheng Zhang
Visualization: Yuhao Wei, Yuanyuan Chen
Writing–original draft: Yuhao Wei, Yuanyuan Chen, Guangqi Li
Writing–review & editing: Xuelei Ma, Yi Zhang, Xiaosheng Zhang, Yi-Ping Ho, Juan Huang

Ethics approval

The animal study was approved by the Ethics Review Committee of Animal Experimentation at West China Hospital, Sichuan University (Approval No. 20240304003). All animal procedures were conducted in strict accordance with the *Guide for the Care and Use of Laboratory Animal*[22]. The human study protocol was reviewed and approved by the Ethics Committee of West China Hospital, Sichuan University (approval ID: 2022_Audit_No. 959), and registered with the Chinese Clinical Trial Registry (Registration number: ChiCTR2300067929). The study was conducted in accordance with the principles of the *Declaration of Helsinki*.[34] Written informed consent was obtained from all participants before enrollment.

Consent for publication

Written informed consent was obtained from all participants for the publication of this study and any accompanying data. All patient data presented in this article have been anonymized, and no identifying details or images of the participants are included.

Availability of data

All data generated or analyzed during this study are included in this published article and its supplementary information files.

Further disclosure

Portions of the findings in this study were previously presented at NUTRITION 2025 (American Society for Nutrition annual meeting), Orange County Convention Center, Orlando, Florida, on June 1, 2025. and published as a conference abstract in *Current Developments in Nutrition* (DOI: 10.1016/j.cdnut.2025.106394). The current manuscript represents the full-length original research with complete experimental details, expanded data analysis, and detailed discussion.

References

1. Horton HR, Moran LA, Scrimgeour KG, Perry MD, Rawn JD. *Principles of Biochemistry*. Pearson College Div; 2006.

2. Latham MC. *Human Nutrition in the Developing World*. Food & Agriculture Organization; 1997.

3. Vettore L, Westbrook RL, Tennant DA. New aspects of amino acid metabolism in cancer. *Br J Cancer*. 2020;122(2):150-156.

   doi: 10.1038/s41416-019-0620-5

4. Lieu EL, Nguyen T, Rhyne S, Kim J. Amino acids in cancer. *Exp Mol Med*. 2020;52(1):15-30.

   doi: 10.1038/s12276-020-0375-3

5. Tong H, Jiang Z, Song L, *et al*. Dual impacts of serine/glycine-free diet in enhancing antitumor immunity and promoting evasion via PD-L1 lactylation. *Cell Metab*. 2024;36(12):2493-2510.e9.

   doi: 10.1016/j.cmet.2024.10.019

6. Choi BH, Coloff JL. The Diverse Functions of Non-Essential Amino Acids in Cancer. *Cancers*. 2019;11(5):675.

   doi: 10.3390/cancers11050675

7. Pant A, Lee AY, Karyappa R, *et al*. 3D food printing of fresh vegetables using food hydrocolloids for dysphagic patients. *Food Hydrocoll*. 2021;114:106546.

   doi: 10.1016/j.foodhyd.2020.106546

8. White PJ, McGarrah RW, Herman MA, Bain JR, Shah SH, Newgard CB. Insulin action, type 2 diabetes, and branched-chain amino acids: A two-way street. *Mol Metab*. 2021;52:101261.

   doi: 10.1016/j.molmet.2021.101261

9. Wu B, Zhao TV, Jin K, *et al*. Mitochondrial aspartate regulates TNF biogenesis and autoimmune tissue inflammation. *Nat Immunol*. 2021;22(12):1551-1562.

   doi: 10.1038/s41590-021-01065-2

10. Ruzzo EK, Capo-Chichi JM, Ben-Zeev B, *et al*. Deficiency of asparagine synthetase causes congenital microcephaly and a progressive form of encephalopathy. *Neuron*. 2013;80(2):429-441.

doi: 10.1016/j.neuron.2013.08.013

11. Ben-Salem S, Gleeson JG, Al-Shamsi AM, *et al*. Asparagine synthetase deficiency detected by whole exome sequencing causes congenital microcephaly, epileptic encephalopathy and psychomotor delay. *Metab Brain Dis*. 2015;30(3):687-694.

doi: 10.1007/s11011-014-9618-0

12. Palmer EE, Hayner J, Sachdev R, *et al*. Asparagine Synthetase Deficiency causes reduced proliferation of cells under conditions of limited asparagine. *Mol Genet Metab*. 2015;116(3):178-186.

doi: 10.1016/j.ymgme.2015.08.007

13. Seidahmed MZ, Salih MA, Abdulbasit OB, *et al*. Hyperekplexia, microcephaly and simplified gyral pattern caused by novel ASNS mutations, case report. *BMC Neurol*. 2016;16:105.

doi: 10.1186/s12883-016-0633-0

14. Gataullina S, Lauer-Zillhardt J, Kaminska A, *et al*. Epileptic Phenotype of Two Siblings with Asparagine Synthesis Deficiency Mimics Neonatal Pyridoxine-Dependent Epilepsy. *Neuropediatrics*. 2016;47(6):399-403.

doi: 10.1055/s-0036-1586222

15. Piao L, Fang YH, Parikh K, Ryan JJ, Toth PT, Archer SL. Cardiac glutaminolysis: a maladaptive cancer metabolism pathway in the right ventricle in pulmonary hypertension. *J Mol Med*. 2013;91(10):1185-1197.

doi: 10.1007/s00109-013-1064-7

16. Newgard CB. Metabolomics and Metabolic Diseases: Where Do We Stand? *Cell Metab*. 2017;25(1):43-56.

doi: 10.1016/j.cmet.2016.09.018

17. Alfadhel M, Alrifai MT, Trujillano D, *et al*. Asparagine Synthetase Deficiency: New Inborn Errors of Metabolism. *JIMD Rep*. 2015;22:11-16.

doi: 10.1007/8904_2014_405

18. Böger RH. The emerging role of asymmetric dimethylarginine as a novel cardiovascular risk factor. *Cardiovasc Res*. 2003;59(4):824-833.

doi: 10.1016/S0008-6363(03)00500-5

19. Wu H, Sang S, Weng P, *et al*. Structural, rheological, and gelling characteristics of starch-based materials in context to 3D food printing applications in precision nutrition. *Compr Rev Food Sci Food Saf*. 2023;22(6):4217-4241.

doi: 10.1111/1541-4337.13217

20. Li J, Ye G, Zhou Z, *et al*. Ultrasound-assisted extraction of polysaccharide from Allium chinense G. Don epidermal waste: Evaluation of extraction mechanism, physicochemical properties, and bioactivities. *Ultrason Sonochem*. 2025;112:107210.

doi: 10.1016/j.ultsonch.2024.107210

21. Zhang Y, Lee AY, Pojchanun K, *et al*. Systematic Engineering approach for optimization of multi-component alternative protein-fortified 3D printing food Ink. *Food Hydrocoll*. 2022;131:107803.

doi: 10.1016/j.foodhyd.2022.107803

22. National Research Council. *Guide for the Care and Use of Laboratory Animals*. 8th ed. National Academies Press; 2011. Available from: https://grants.nih.gov/grants/olaw/guide-for-the-care-and-use-of-laboratory-animals.pdf

23. Park KD, Kim TH, Lee SH. The Gugging Swallowing Screen in dysphagia screening for patients with stroke: A systematic review. *Int J Nurs Stud*. 2020;107:103588.

doi: 10.1016/j.ijnurstu.2020.103588

24. Estupiñán Artiles C, Regan J, Donnellan C. Dysphagia screening in residential care settings: A scoping review. *Int J Nurs Stud*. 2021;114:103813.

doi: 10.1016/j.ijnurstu.2020.103813

25. Wang J, Li J, Zeng D, *et al*. Comprehensive evaluation of extraction process, physicochemical properties and bioactivities of hawk tea polysaccharides: comparison of ultrasonic and hot water extraction. *Ultrason Sonochem*. 2025;120:107477.

doi: 10.1016/j.ultsonch.2025.107477

26. Ye G, Li J, Wang J, *et al*. Advantages of ultrasonic-assisted extraction over hot water extraction for polysaccharides from waste stems of Rubia cordifolia L.: A comprehensive comparison of efficiency, structure, and bioactivity. *Ultrason Sonochem*. 2025;120:107502.

doi: 10.1016/j.ultsonch.2025.107502

27. Liu L, Yang X, Bhandari B, Meng Y, Prakash S. Optimization of the Formulation and Properties of 3D-Printed Complex Egg White Protein Objects. *Foods*. 2020;9(2):164.

doi: 10.3390/foods9020164

28. Nasser J, Mehravar S, Pimentel M, *et al*. Elemental Diet as a Therapeutic Modality: A Comprehensive Review. *Dig Dis Sci*. 2024;69(9):3344-3360.

doi: 10.1007/s10620-024-08543-1

29. Rodríguez-Hernández AK, Pérez-Martínez JD, Gallegos-Infante JA, Toro-Vazquez JF, Ornelas-Paz JJ. Rheological properties of ethyl cellulose-monoglyceride-candelilla wax oleogel vis-a-vis edible shortenings. *Carbohydr Polym*. 2021;252:117171.

doi: 10.1016/j.carbpol.2020.117171

30. Cichero JA, Lam P, Steele CM, *et al*. Development of International Terminology and Definitions for Texture-Modified Foods and Thickened Fluids Used in Dysphagia Management: The IDDSI Framework. *Dysphagia*. 2017;32(2):293-314.

doi: 10.1007/s00455-016-9758-y

31. Dick A, Bhandari B, Dong X, Prakash S. Feasibility study of hydrocolloid incorporated 3D printed pork as dysphagia food. *Food Hydrocoll*. 2020;107:105940.

    doi: 10.1016/j.foodhyd.2020.105940

32. Tian Z, Zhong Q, Zhang H, *et al*. Optimising printing fidelity of the single-nozzle based multimaterial direct ink writing for 3D food printing. *Virtual Phys Prototyp*. 2024;19(1):e2352075.

    doi: 10.1080/17452759.2024.2352075

33. Maldonado-Rosas R, Pérez-Castillo JL, Cuan-Urquizo E, Tejada-Ortigoza V. The role of controlled voids shape on the flexural properties of 3D printed food: an approach for tailoring their mechanical properties. *Virtual Phys Prototyp*. 2024;19(1):e2284816.

    doi: 10.1080/17452759.2023.2284816

34. World Medical Association. Declaration of Helsinki: ethical principles for medical research involving human subjects. *JAMA*. 2013;310(20):2191-2194.

    doi: 10.1001/jama.2013.281053